Solids sampling using double-pulse laser ablation inductively coupled plasma mass spectrometry.

Jhanis González, Chunyi Liu, Jong Yoo, Xianglei Mao and Rick Russo*

Lawrence Berkeley National Laboratory, Berkeley, CA 94720, USA

*Corresponding author. Tel.: +1-510-486-4258; fax: +1-510-483-7303. rerusso@lbl.gov

Abstract

This paper describes the use of double-pulse laser ablation to improve ICP-MS internal precision (temporal relative standard deviation, %TRSD). Double pulse laser ablation offers reduced fractionation, increased sensitivity, and improved signal to noise ratios. The first pulse is used to ablate a large quantity of mass from the sample surface. The second pulse is applied with a variable time delay after the first pulse to break the ablated mass into a finer aerosol, which is more readily transported to and digested in the ICP-MS.

Keywords: Double pulse mode; Laser ablation; ICP-MS; particles break down

Introduction

Continuous pulsing at one spot on a sample is commonly used in laser ablation chemical analysis to improve analytical precision[1;2]. However, fractionation induced by crater formation (aspect ratio of the crater depth and diameter) can occur during continuous pulsing [3]. In contrast to continuous pulsing, single pulse laser ablation avoids fractionation related to crater formation. In addition, single pulse analysis is suitable for spatial resolution or depth profile analysis, such as analysis of inclusions and thin films. There are several concerns with single pulse ablation, including poor measurement reproducibility (external precision), small quantity of ablated mass inducing weak ICP-MS intensity, and single-pulse elemental fractionation. Due to the transient nature of single-pulse ablation and sequential collection by quadrupole mass filters, which are commonly used in ICP-MS, element signals may be lost during multi-elemental analysis, causing poor measurement precision (internal precision)[4]. Although the use of the time of flight mass spectrometer (TOF-MS) for the measurements of transit signals (as single pulse laser ablation sampling) is increasing due to its simultaneous collection for all elements, quadrupole mass detectors are still suitable for single pulse ablation if the data acquisition parameters and number of elements are reasonably arranged (<20 elements to be analyze, dwell time, etc.)[4].

In order to increase the amount of ablated mass and avoid low ICP-MS intensity, a phase explosion process can be use to significantly enhance mass removal[5]. In phase explosion, rapid heating of the sample generates a superheated liquid layer and subsequent homogeneous nucleation within the heated layer causes violent ejection of mass. However the large quantity of material removed by phase explosion produces a wide range of particles sizes, which will influence ICP-MS internal precision and fractionation[6;7]. In general, large particles can cause problems in LA-ICP analysis,

primarily because of inefficient mass transport, and if they reach the ICP, incomplete digestion [9-12]. The chemical composition of particles produced from laser ablation is related to particle size, however the overall composition of the produced particles represent the bulk composition[8]. Achieving a smaller particle size distribution is important in general, but particularly for single pulse analyses where the signal intensity and quality will depend on the ablated material transport efficiency and its digestion by the ICP.

The use of filters to eliminate large particles improves elemental fractionation and accuracy[10]. However, this approach can result in a large loss of material, which in case of small samples can not be afforded. In order to generate small particles, many groups have varied laser ablation parameters such as laser energy, spot size, pulse width, wavelength, the gas environment, etc [9;12;13]. In general, the use of UV wavelengths, shorter pulse durations, and helium as the chamber gas improves the production of small particles.

The basis of this work was to apply a second laser pulse after a delay time to break large ablated particles into a finer aerosol. Effective break-up of large particles by the second laser pulse can result in improved accuracy of chemical sampling. The use of a second pulse provides better temporal signal precision (internal precision) in the form of lower temporal relative standard deviation (TRSD).

Experimental

The experiments were performed using a 266nm laser (Solo-PIV, New wave research) with sampling into an ICP-MS (VG PQ3). The ablation was performed in an argon environment. The solo PIV laser has two collinear 266nm beams arising from two laser heads mounted on a single base plate. The beams share the same light path to a fourth harmonic generator. The time between pulses from the two laser heads was achieved by using a delay generator (Stanford Research System Inc. Model DG535); the delay could be change from nanoseconds to several seconds.

The sample was brass with a composition of copper (Cu) of 51.48% and zinc (Zn) of 48.52%. The polished brass sample was placed in an ablation chamber where the laser beams were focused to a spot size of ~ 40μm, and the energy was set to induce phase explosion from the sample surface. All experimental parameters are listed in table 1.

Three positions on the sample were ablated for each delay time between the two lasers. For each sample position, the signal intensity versus delay time and the relative standard deviation were calculated from the ICP-MS data. The crater volumes were measured using a White light interferometric microscope (Zygo 200).

The ejection of particles from the sample surface also was monitored using time-resolved shadowgraph imaging. A schematic of the imaging system is shown in figure 1. A Spectra-Physics TSA laser with pulse duration of approximately 100 femtosecond (full width at half maximum), is used as a probe beam that is perpendicular to the ablation laser beam. The probe beam is directed to a charge coupled device (CCD) camera after passing through a narrowband 400 nm filter. By changing the delay time, the probe beam can be varied in time with respect to the ablation beam.

Results and Discussions

It is common to observe spikes in the ICP-MS temporal response during laser ablation sampling; these spikes originate from large ablated particles and not due to instrumental noise[14;15]. Due to the sample residence time in the ICP, only one particle can be detected during each element isotope sweep with quadrupole instruments. The spikes will generate errors when determining the temporal ratio of two elements.

We used a double laser pulse approach to break large particles, providing a narrower particle size distribution. Figure 2 shows the temporal signal intensity of both ^{65}Cu (*a,c*) and ^{66}Zn (*b,d*) from the brass sample at two different delay times (2μsec and 1sec). Higher intensity response is observed for delay time of 2 μseconds between lasers pulses compare to 1 second. In addition there are a higher number of spikes for a delay time of 1 second compared to 2 μseconds. Calculation of the temporal relative standard deviation (TRSD), related to a short term change in the temporal signal, shows the improvement in performance:

$$S_i = \frac{1}{5}\sum_{j=1}^{5} X_{i-3+j} \qquad \textbf{(1)}$$

$$E_i = X_i - S_i \qquad \textbf{(2)}$$

$$\%TRSD = \left(\frac{\frac{1}{\sqrt{n-1}}\left(\sum_{i=1}^{n} \sqrt{\left(E_i - \overline{E}_0\right)^2} \right)}{\frac{1}{n}\sum_{i=1}^{n} X_i} \right) * 100 \qquad \textbf{(3)}$$

First the signal was smoothed using equation *1*, and then the error was calculated as the difference between the original temporal signal X_i and the smooth signal S_i,

using *2*. Finally, the temporal relative standard deviation was calculated using equation *3*, where $\frac{1}{n}\sum_{i=1}^{n} X_i$ is the integrated temporal signal.

The data obtained for ^{65}Cu using the above formulas are presented in figure 3. The error bars represent the error between three different experiments (external precision). The TRSD and external precision are optimized for a delay times in the microsecond range, which corresponds to minimum spikes in the temporal signal. This reduction in the number of spikes for the microsecond delay can be attributed to break-up of large particles by the second laser pulse.

The ^{66}Zn signal had fewer spikes than ^{65}Cu. Liu et al.[17] showed that the spikes were element dependent and had a close correlation with elemental thermal properties. (Table 2 shows Cu and Zn properties). In recent work by Jaworski et. al.[8] using brass samples the copper composition increased for particles with an aerodynamics diameter in the range of 0.1 and 1.5μm while the content of zinc decreased in the same diameter range. It was establish that Zn signals were related to smaller particles while Cu signals were related to larger particles.

The ICP-MS integrated response versus delay time between laser pulses for ^{65}Cu is shown in figure 4*a*; the error bars represent the standard deviation of three replicates. An increase in the total signal intensity was measured for delay times between 100ns-5μs compare to a 1 second delay time. The use of 1 second delay time represents the case where two separate pulses are used for ablation[17]. The interaction between the second pulse and the mass ablated by the first pulse is negligible at 1 second delay. Normalization of the integrated signal for each delay time to the integrated signal obtained for 1 second delay shows an increase between 1.5-2.0 times (figure insert 4*a*). Volume measurements were performed to determine if the increase in the signal intensity was due to an increase in the ablated mass. Figure 4*b* shows the normalized net

volumes by the measurement of 1 second. The crater volume increase by 20% in the microsecond range, which does not justify the increase in signal intensity (50-100% respect to 1s data). The improvement in the signal intensity and the decreased appearance of spikes in the temporal signal is mainly attributed to breaking up particles by the second laser pulse.

The performance improvement will be related to the coupling of the second laser pulse with the ablated particles. If the energy from the second laser pulse is absorbed by the ablated material, the process should be more efficient. If this is not the case, the second pulse will directly ablate the sample, producing additional large particles. If the ablated particles are not all ejected from the sample perpendicular to the surface; the interaction between the second pulse with the ablated particles is reduced. Effective break-up of ablated particles can be achieve by optimizing the second pulse parameters such as; pulse width (allowing longer interaction with the ablated material), spot size (i.e. larger spot size to allow interaction with the particles that are not ejected perpendicular to the sample); laser energy, etc. These parameters were not adjustable with the laser used in this work.

Shadowgraph images measured perpendicular to the surface after single and double pulse are presented in figure 5. Figure 5*a* shows the ablated mass 400 nanoseconds after the first laser pulse, ejecting from the sample in a conical shape. Figure 5*b* shows an image taking 50ns after the second pulse (total time after the first pulse 450ns); showing the change in initial particles. Compared to individual particles spreading everywhere in single pulse case, it can be noticed that a dense cloud was formed, which is suspected to be vapor of the breaking particles dissociated by the second pulse. Figure 5*c* shows an image 396 ns after the second pulse (total time after the first pulse 796ns); this image shows how the second pulse is also generating

particles from the sample, with a larger particles size, which could minimized its effect on the first particles. It is also possible that some particles were missed by the second pulse if their travel trajectory was outside its path. In this case the use of the second pulse perpendicular to the first pulse it could help to improve the particle breaking efficiency.

Conclusion

Double pulse laser ablation sampling with ICP-MS can be used to improve the temporal stability (internal) and the external precision of analysis.

The way the ablated material leaves the sample is a very important parameter to evaluate during this experiments, the fact that the ablated material does not comes out perpendicular to the surface limited the second pulse interaction with it. These preliminary results, however, reveal the importance of further investigation on the performance by the second pulse over the particles. Future work will investigate more depth the effect of the optimization of second pulse parameters such as: pulse width, energy, spot size, etc.

The temporal relative standard deviation (TRSD) shows a lower value between 100ns-5μs delay time range, meaning that the number of spikes on the transient signal were minimized in this range of delay time between pulses which is relating to breaking of large particles by the second pulse.

Acknowledgements

This research was supported by the U.S. Department of Energy, Office of Nonproliferation and National Security (NA22), at the Lawrence Berkeley National Laboratory, under Contract No. DE-AC03-76SF00098.

Reference List

1. Gunther, D.; Jackson, S. E.; Longerich, H. P. *Spectrochim.Acta Pt.B-At.Spec.* **1999,** *V54*, 381-409.

2. Russo R.E.; Mao, X. L.; Liu, H. C.; Gonzalez, J.; Mao, S. S. *Talanta* **2002,** *V57*, 425-51.

3. Mank, A. J. G.; Mason, P. R. D. *J.Anal.Atom.Spectrom.* **1999,** *V14*, 1143-53.

4. Pettke, T.; Heinrich, C. A.; Ciocan, A. C.; Gunther, D. *J.Anal.Atom.Spectrom.* **2000,** *V15*, 1149-55.

5. Yoo, J. H.; Borisov, O. V.; Mao, X. L.; Russo, R. E. *Anal.Chem.* **2001,** *V73*, 2288-93.

6. Koch J.; Feldmann I.; Jakubowski N.; Niemax K. *Spectrochim.Acta Pt.B-At.Spec.* **2002,** *57*, 975-85.

7. Figg, D. J.; Cross, J. B.; Brink, C. *Appl.Surf.Sci.* **1998,** *127-129*, 287-91.

8. Jaworski R.; Hoffmann, E.; Stephanowitz H. *International Journal of Mass Spectrometry* **2002,** *219*, 373-79.

9. Horn I; Gunther, D. *Appl.Surf.Sci.* **2003,** *207*, 144-57.

10. Guillong, M.; Kuhn H-R; Gunther, D. *Spectrochim.Acta Pt.B-At.Spec.* **2003,** *58*, 211-20.

11. Guillong, M.; Gunther, D. *J.Anal.Atom.Spectrom.* **2002**.

12. Jeong, S. H.; Borisov, O. V.; Yoo, J. H.; Mao, X. L.; Russo, A. E. *Anal.Chem.* **1999,** *71*, 5123-30.

13. Guillong, M.; Horn I; Gunther, D. *J.Anal.Atom.Spectrom.* **2003,** *18*, 1224-30.

14. Outridge, P. M.; Doherty, W.; Gregoire, D. C. *Spectrochim.Acta Pt.B-At.Spec.* **1996,** *V51*, 1451-62.

15. Aeschliman, D. B.; Bajic S.J.; Baldwin D.P.; Houk, R. S. *J.Anal.Atom.Spectrom.* **2003,** *18*, 1008-14.

16. Bleiner, D.; Gunther, D. *J.Anal.Atom.Spectrom.* **2001,** *16*, 449-56.

17. Liu, H. C.; Mao, X. L.; Russo, R. E. *J.Anal.Atom.Spectrom.* **2001,** *16*, 1115-20.

Table 1: Experimental conditions.

Laser Ablation Device	*New Wave Research. Solo-PIV*
Nd:YAG	266nm
	4 ns pulse length
Energy	2.7 mJ
Spot size on the sample	40 μm
Fluence	150 J/cm^2
ICP-MS	*PQ3, VG-Elemental*
Detector	Simultaneous mode detector
ICP-MS Parameters	
RF power	1300 W
Plasma Ar gas flow rate	14.2 L/min
Auxiliary Ar gas flow rate	1.02 L/min
Carrier Ar flow rate	1.3 L/min
ICP-MS Dwell time	10 ms
Data acquisition mode	Time resolved (TRA)

Table 2: Sample composition

Brass	%	Melting Temperature ºC	Boiling Temperature ºC	Heat of Fusion (kJ/mol)
Cu	**51.48**	**1083**	**2567**	**13.050**
Zn	**48.52**	**419.58**	**907**	**7.322**

Figure captions

Figure 1: Time-resolved shadowgraph imaging system.

Figure 2: Temporal signal intensity of both ^{65}Cu (*a,c*) and ^{66}Zn (*b,d*) from the brass sample at 2μsec and 1sec delay times.

Figure 3: Temporal relative standard deviation for ^{65}Cu versus delay time between pulses.

Figure 4: a) Integrated **s**ignals for ^{65}Cu versus delay time between pulses. (Insert plot: Integrated signals for ^{65}Cu normalized by the signal of 1sec) **b)** Normalized net volumes by the volume of 1 second delay time.

Figure 5: a) Material coming out the sample after 400 ns of the first pulse. **b)** Image taking 50ns after the second pulse. **c)** Image taking 396 ns after the second pulse.

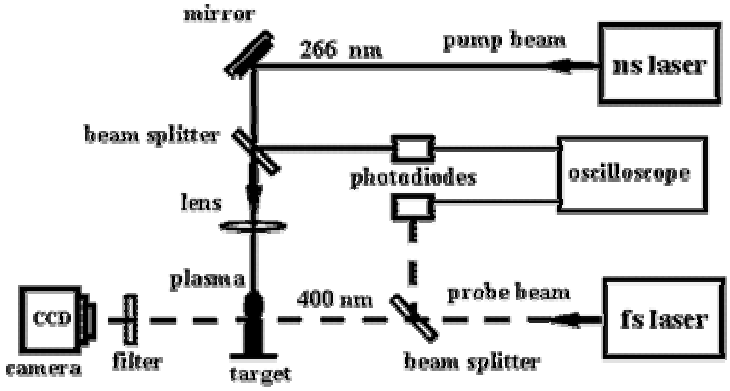
mirror
266 nm
pump beam
ns laser
beam splitter
photodiodes
oscilloscope
lens
plasma
400 nm
probe beam
fs laser
CCD
camera
filter
target
beam splitter

Figure 1

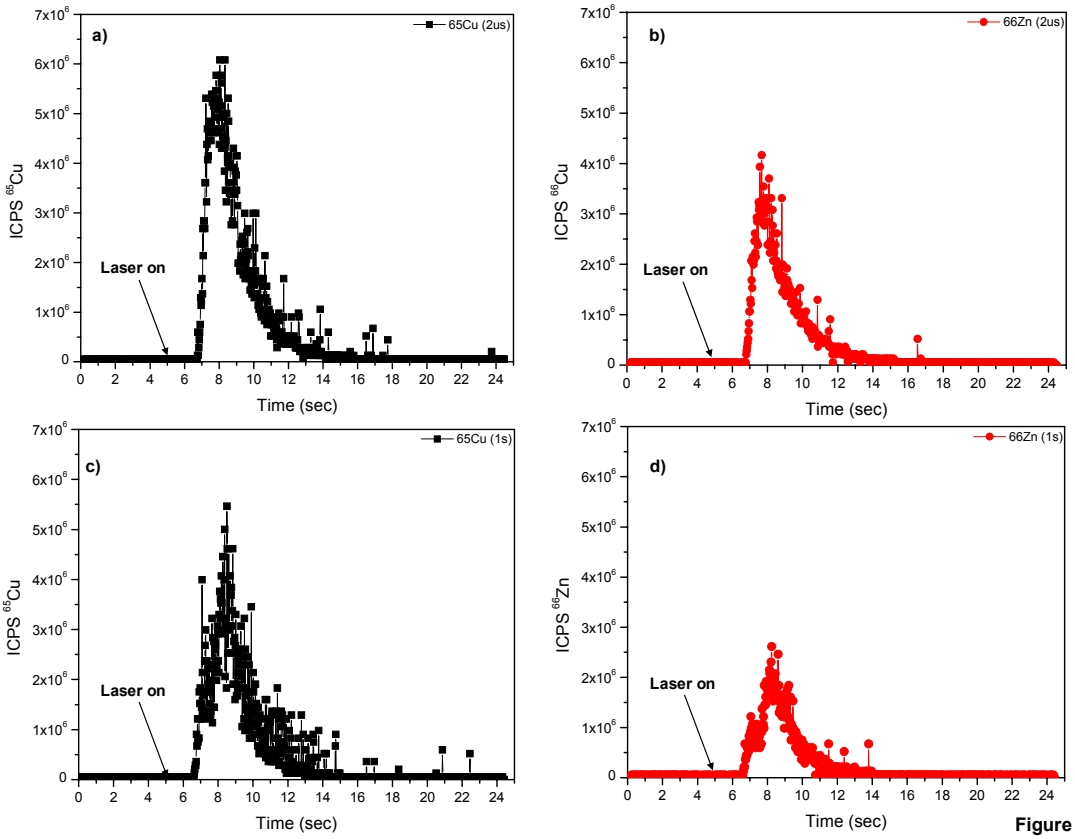
a)
65Cu (2us)
ICPS 65Cu
Laser on
Time (sec)
b)
66Zn (2us)
ICPS 66Cu
Laser on
Time (sec)
c)
65Cu (1s)
ICPS 65Cu
Laser on
Time (sec)
d)
66Zn (1s)
ICPS 66Zn
Laser on
Time (sec)

Figure 2

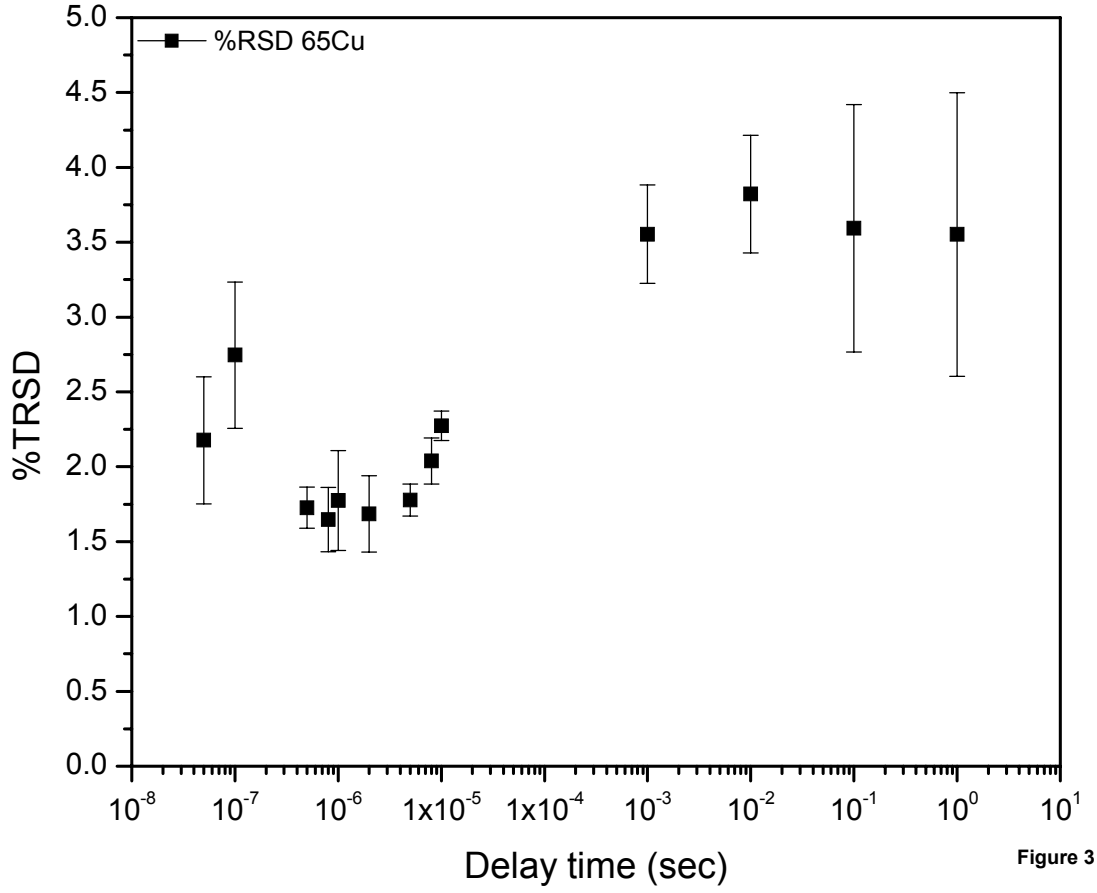
%RSD 65Cu
%TRSD
5.0
4.5
4.0
3.5
3.0
2.5
2.0
1.5
1.0
0.5
0.0
10-8
10-7
10-6
1x10-5
1x10-4
10-3
10-2
10-1
100
101
Delay time (sec)

Figure 3

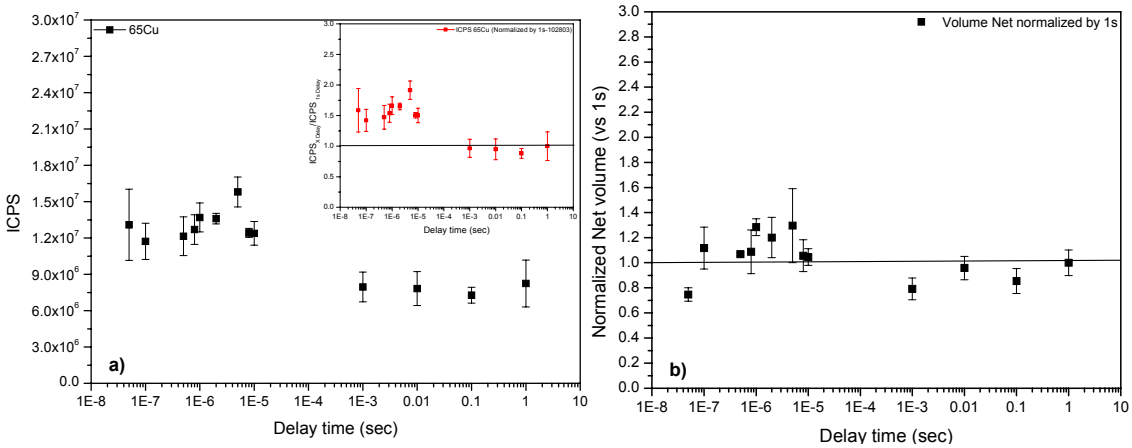
65Cu
ICPS
Delay time (sec)
a)
ICPS 65Cu (Normalized by 1s-102803)
Volume Net normalized by 1s
Normalized Net volume (vs 1s)
b)

Figure 4

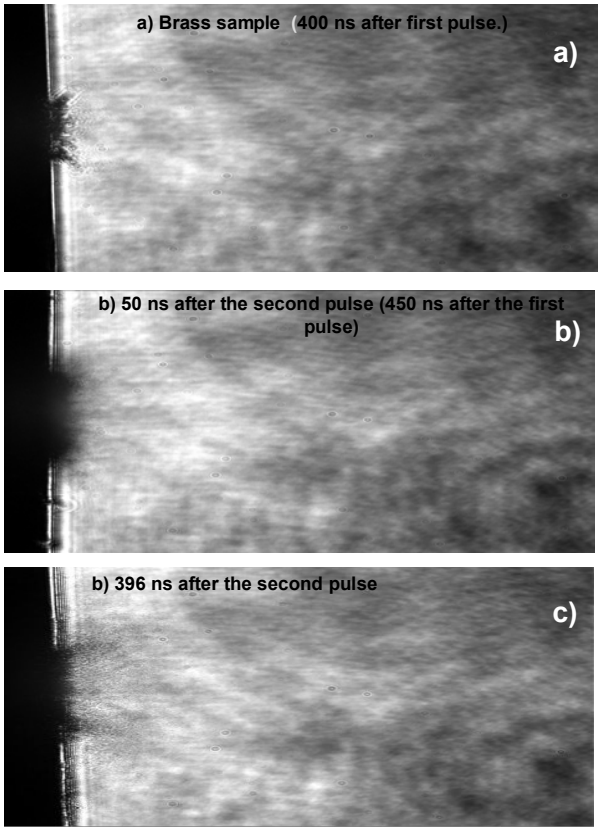
a) Brass sample (400 ns after first pulse.)
a)
b) 50 ns after the second pulse (450 ns after the first pulse)
b)
b) 396 ns after the second pulse
c)

Figure 5